Applied Physics Letters

Nano-second time resolved investigations on thermal implications of high-field transport through MWCNTs

Cite as: Appl. Phys. Lett. **110**, 233111 (2017); https://doi.org/10.1063/1.4984282
Submitted: 07 February 2017 • Accepted: 16 May 2017 • Published Online: 07 June 2017

Abhishek Mishra, Ravi Nandan, Srinivasan Raghavan, et al.

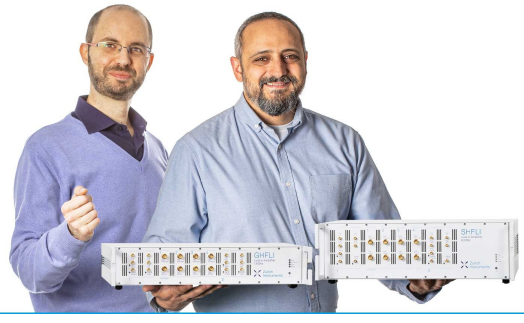

AIP Publishing

Nano-second time resolved investigations on thermal implications of high-field transport through MWCNTs

Abhishek Mishra,[1,2,a)] Ravi Nandan,[3] Srinivasan Raghavan,[2] and Mayank Shrivastava[1]
[1]*Department of Electronic Systems Engineering, Indian Institute of Science, Bangalore 560012, India*
[2]*Centre for Nano Science and Engineering, Indian Institute of Science, Bangalore 560012, India*
[3]*Materials Research Centre, Indian Institute of Science, Bangalore 560012, India*

(Received 7 February 2017; accepted 16 May 2017; published online 7 June 2017)

The high-current carrying capacity of Multi-walled Carbon Nanotubes (MWCNTs) is the central idea behind their possible applications as interconnects. Joule-heating due to transport of high current through constricted quasi-1D electron channel results in various temperature-driven phenomena. Two such phenomena are current annealing and irreversible breakdown, which play vital roles in deciding electron transport and interconnect reliability, respectively. These phenomena occur at the time scale of 1–100 ns and hence cannot be precisely captured by conventional steady-state or DC measurement techniques. In this work, we explore these two phenomena by investigating electro-thermal transport through the inner and outer shells of MWCNTs, both suspended and substrate-supported, at the time scale of nano-seconds. *Published by AIP Publishing.*
[http://dx.doi.org/10.1063/1.4984282]

Multi-walled Carbon Nanotubes (MWCNTs)[1] have been widely investigated and are known for their extraordinary current carrying capacity. Conduction of current as high as 10^9 A/cm^2 has been reported previously.[2,3] Although this feature makes them suitable for interconnect applications in integrated circuits, it also results in excessive self-heating of the tube. Self-heating is the physical manifestation of an increase in population of optical phonons due to inelastic scattering of energetic electrons by lattice atoms.[4] The optical phonons are high-energy modes of lattice vibrations, which in turn makes the self-heating a high-field phenomenon. Self-heating results in various variability and reliability issues like annealing[5–9] and breakdown,[10,11] respectively. Although these two issues have been successfully reported in the past, their analysis is still limited due to sudden breakdown of the tubes under high-field conditions. Moreover, these earlier studies are based on DC measurements or steady-state analysis. Such an analysis extracts I-V signatures from devices under equilibrium and hence reports post-event or failure signatures. However, given the nature of temperature driven events, the analysis of the non-equilibrium state is expected to uncover the exact, time resolved mechanism and offer deeper insights into annealing and breakdown of MWCNTs.

The above discussion calls for re-investigation of high-field transport through MWCNTs during the non-equilibrium state. In general, the duration of a thermal non-equilibrium state is characterized by thermal diffusion time, during which heat travels from hot regions to cold regions of the device. For a MWCNT with length L and thermal diffusivity α, the thermal diffusion time is given by $L^2/\pi^2\alpha$. Hence, in a micron long tube with thermal diffusivity of the order of 10^{-5} m^2/s,[12,13] phonon transport from hot contact to cold contact would take few tens of nano-seconds. Therefore, probing and sensing the electrical transport through the tube, which is limited to few tens of nano-seconds and sampled at the timescale of sub-ns, not only control the self-heating and early failure but also can give subtle information on electro-thermal transport under thermal non-equilibrium. It is worth highlighting that this time-scale also corresponds to the switching frequency (1 GHz) of state-of-the-art CMOS circuits.[14] Hence, for the deployment of CNTs in high-frequency applications, the performance and reliability assessment should be done at the time-scale of nano-seconds. Keeping the above discussion in mind, in this work, we have developed and demonstrated a technique for nano-second time resolved investigations of non-equilibrium phenomena such as annealing and MWCNT shell breakdown. The investigations monitored at sub-ns time scales and limited to few tens of nano-seconds have allowed probing the electro-thermal transport and associated events without leading to early failure or breakdown.

Figure 1 shows the nano-second pulse setup used for investigations in this work. For investigating the change in MWCNT's characteristics after every nano-second pulse, a current-voltage (I-V) measurement unit (source measure unit or SMU) is integrated with the setup, which measured low-field DC characteristics of the device after each pulse. A measurement routine consists of applying a series of alternate voltage pulses with increasing amplitude and low DC voltages of fixed amplitude across the device. Unless specified otherwise, a pulse I-V sweep with a pulse width of 50 ns is executed first, followed by 100, 150, and 250 ns. This is to ensure a gradual increase in joule heating across the device. To study the role of individual shells, devices used in the work are realized to have top-contacted electrodes, wherein only the outermost shell contacts the metal and inner concentric shells participate in conduction via tunneling[15] till the outermost shell is not broken. Since the tunneling probability increases with the applied field, participation of inner shells, and hence the conductance of the device, increases with increasing pulse amplitude. The high-field transport enabled by nano-second time resolved investigations allow conduction through both inner and outer shells, whereas the low-field DC allows conduction

a)Electronic mail: abhishekmishra@dese.iisc.ernet.in

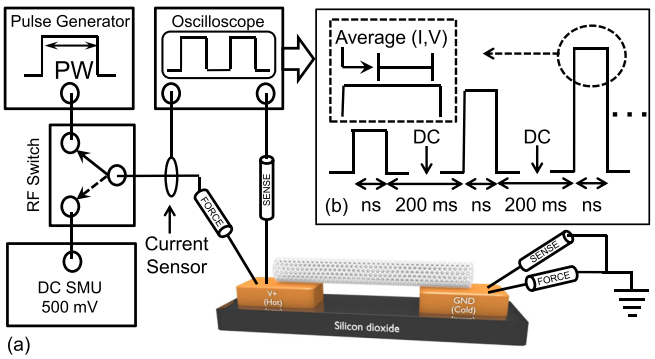

FIG. 1. (a) Pulse generator coupled with a suspended MWCNT through 50 Ω RF probes arranged in a four probe fashion. The pulse current is sensed using a 1 GHz inductive current sensor. Both the voltage and current waveforms were captured by using a digital storage oscilloscope (25 GS/s). An RF switch is integrated between the pulse generator and SMU for low-bias DC (0.5 V) measurement after each pulse. (b) I-V data point corresponding to a given applied pulse is extracted by averaging the I-V waveform from 70% to 90% of the pulse width. The pulse-to-pulse delay is set to 200 ms to ensure sufficient time for the device to cool down to ambient temperature.

only through outer shells. This has allowed us to compare a device's resistance attributed to the outer shell with the total resistance. Devices used in this work were fabricated using dielectrophoresis[16] of the MWCNT suspension over palladium electrodes, which in turn were patterned by e-beam lithography.

Figure 2(a) shows pulse I-V characteristics and device resistance of a 500 nm long suspended MWCNT, extracted by executing the pulse I-V measurement routine, as described

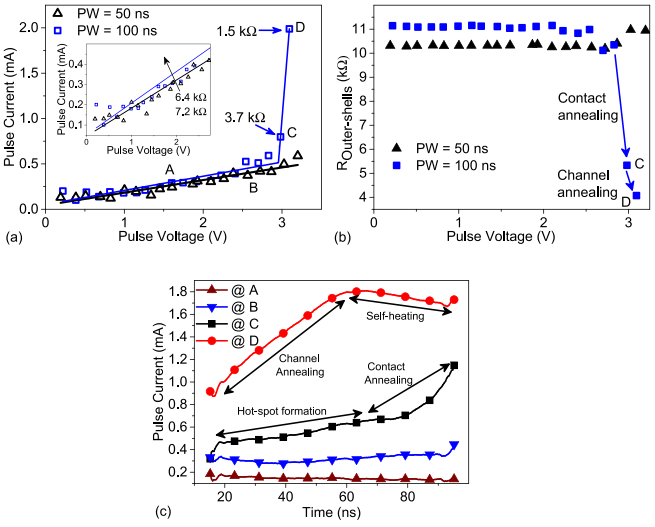

FIG. 2. Response of a 500 nm long suspended MWCNT towards nano-second charge bursts. (a) The device shows linear pulse I-V characteristics for a pulse width of 50 ns, while that for 100 ns shows an abrupt jump in current and a fall in the resistance beyond a critical voltage. The inset shows the low-bias resistance of the un-annealed tube and highlights a meager change in the resistance at low pulse voltages. (b) Depicts current annealing of the device. The resistance of outer-shells was measured by applying low-bias DC to the device after stressing through nano-second time resolved pulses. A fall in the resistance of outer-shells confirms annealing by 100 ns long pulses. Note that the contact and channel annealing are differentiated by the investigation of the low-bias resistance. Compared to channel annealing, the contact annealing results in a relatively more reduction in the low-bias resistance. (c) Transient waveforms at the points marked in (a) show annealing at the nano-second time scale. A single current-voltage value corresponding to a transient waveform is extracted by averaging the transient data from 70% to 90%. A pictorial representation of the same is given in Fig. 1(b).

above, with two different pulse widths. Pulse I-V with 50 ns wide pulses results in linear I-V characteristics, even at higher voltages, which indicates the fixed device resistance and no change even at higher powers. Moreover, the outer-shell resistance, extracted after each pulse, does not show any pulse-to-pulse variation. In contrast to this, the pulse I-V measurement with 100 ns wide pulses shows an abrupt non-linear increase in current [Fig. 2(a)] and sudden fall in the total resistance [Fig. 2(a)] and post pulse extracted outer shell resistance [Fig. 2(b)]. As mentioned earlier, the low-bias DC resistance is extracted between two consecutive pulses and consists of the resistance of outer-shells and CNT-metal interface. These observations indicate that the permanent reduction in the outer-shell resistance, which is attributed to current-annealing,[17] requires a certain power and takes place after a certain time, which is 50 ns in the present case. As discussed earlier, the conductance of a side-contacted MWCNT increases with applied voltage. In contrast to this, the I-V characteristics for measurements done with 50 ns wide pulses show the constant resistance [Fig. 2(a)], which indicates the absence of tunneling and the presence of a large tunneling barrier at the nanotube-metal interface. This tunneling barrier could be because of adsorbents trapped between the nanotube and the metal[18] [Fig. 3(a)], which weakens the interaction between atomic orbitals of the metal and carbon atoms. The reduction of both these sources of the barrier requires scattering-induced heating of the interface for a sufficient amount of time. Transient waveforms corresponding to four different pulse voltages shown in Fig. 2(c) reveal that scattering-induced heating for more than 50 ns is required to maintain the hot-spot and initiate the current-annealing. The large metal electrode beneath the MWCNT takes away a huge fraction of the heat generated and delays the formation of hot-spots. Transient waveforms [Fig. 2(c)] corresponding to points *A* and *B* in Fig. 2(a) do not show any time-dependent increase in current, while the waveforms corresponding to points *C* and *D* show an increase in current with time. Point C marks the initiation of current annealing, at which the device shows a transient increase in current followed by a decrease in the outer-shell resistance from 10 kΩ to 5.5 kΩ [Fig. 2(b)]. The immediate next pulse, which corresponds to point *D*, shows a further increase in current with respect to time; however, unlike *C*, this time, the rise starts earlier. Although the pulse corresponding to point *D* injects more

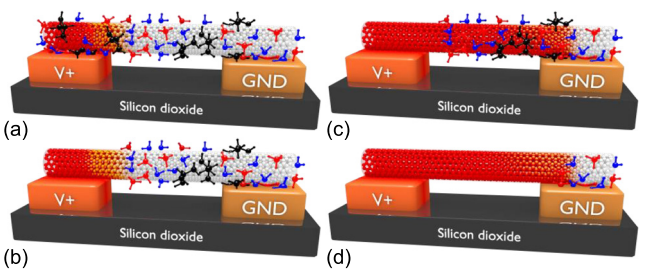

FIG. 3. Sequence of events contributing to annealing of a suspended MWCNT. (a) Electron-phonon scattering at the hot electrode (*V*+), which forms a hot-spot; (b) the hot-spot de-adsorbs the adsorbed molecules and anneals the contacts; (c) rise in current due to contact annealing populates optical phonon modes in the channel and results in an increase in channel temperature; and (d) desorption of adsorbed molecules from the channel follows the rise in temperature.

energy into the device, the outer-shell resistance drops by 1.5 kΩ only [Fig. 2(b)], which is a relatively less reduction compared to the previous pulse.

We further investigate the above observations through the schematic of the annealing sequence shown in Fig. 3. The metal-CNT interface and the channel of the as-fabricated device host a variety of adsorbents due to the fabrication process and ambient atmosphere. Adsorbents at the interface increase the contact resistance. Consequently, before annealing of contacts, a major fraction of applied voltage drops across the metal-CNT interface and a relatively smaller voltage drops across the channel. Consequently, most of the scattering and subsequent heating occur at the contacts [Fig. 3(a)]. The local heating of the metal-CNT interface results in the desorption of adsorbents and subsequent formation of carbide.[5] Both these processes result in a significant reduction in the contact resistance [Fig. 3(b)]. Post contact-annealing [Fig. 3(c)], reduction in the contact resistance lowers the voltage drop across the metal-CNT interface, which in turn increases the electric-field across the channel. A high electric-field across the channel populates optical phonon modes, which eventually causes local-heating throughout the channel. An increase in channel temperature releases the adsorbed molecules and results in the annealing of the channel [Fig. 3(d)]. Note that channel annealing decreases the resistance of the outermost shell only, while annealing of the interface reduces the contact resistance of the entire MWCNT. Consequently, the former process of annealing results in a relatively lower reduction in the resistance than the latter process. It is worth highlighting that tunneling current across the metal-insulator-metal junction, MWCNT-air-metal in the present case, depends on the thickness of the barrier. Analytically, the tunneling current is given by $I \sim \exp^{-2\kappa d}$, where $\kappa = \sqrt{2m\phi}/h$ and d is the tunneling distance, while ϕ is the barrier height. The expression suggests an exponential rise in current with reduction in the tunneling distance, which further corroborates the increase in current through MWCNTs with desorption of adsorbents from the metal-MWCNT interface.[19] Furthermore, the nano-second analysis reveals, as depicted in Fig. 2(c), that compared to contact annealing, the channel annealing is relatively a faster process and occurs simultaneously with channel self-heating. This difference arises due to the rate at which phonon population increases across the metal-CNT interface, compared to the channel. As discussed earlier, the presence of metal pads (heat-sink) slows down the self-heating or phonon population and delays the formation of hot-spots, which in turn results in time-delay associated with contact annealing. In contrast to this mechanism, self-heating in the channel is due to remote joule heating[20] and electron-phonon scattering in the channel, which leads to high-energy slow-decaying optical phonons. At higher electric fields, such phonon modes populate the entire channel and results in annealing of the channel. Before annealing of the contacts, electron-phonon scattering takes place at the contact, which however, after contact annealing, shifts to the MWCNT channel.[21] Another aspect that attributes to this phenomenon is the increase in current flow through the channel after contact annealing, which in turn increases phonon population. Increased phonon population results in the desorption of surface adsorbents[22] and subsequent annealing of the channel. Note that at high pulse voltages, the channel current initially increases due to contact and channel annealing and then decreases monotonically after maxima, which signifies mobility degradation due to increased electron-phonon scattering or the reduced mean scattering length. Note that the similar behavior of annealing, i.e., channel annealing preceded by contact annealing, will be observed if bias-voltage corresponding to *D* is applied before *C*. This is because the channel annealing requires the emission of optical phonons, which in turn requires field-assisted generation of hot carriers. In devices with un-annealed contacts, most of the voltage drop occurs at the metal-MWCNT interface, due to which the channel remains devoid of high electric-fields and optical phonons. Post contact annealing, a high electric field develops across the channel, which in turn dissipates heat due to generation of optical phonons, and causes annealing of the channel.

In order to check the effectiveness and extent of annealing done using 100 ns long pulses, the measurement routine was executed with a pulse width of 150 ns. The increase in thermal energy through 150 ns pulses did not show any permanent change in the resistance of outer shells (see Fig. S1 in the supplementary material), indicating that the device is completely annealed through 100 ns pulses. In the next cycle of the measurements, the pulse width was increased to 250 ns to cause slow and observable breakdown of the tube. Both the pulse I-V and outer-shell resistance (Fig. 4) show abrupt failure. The transient current waveform [Fig. 4(c)] depicts a gradual fall in the current after 75 ns followed by abrupt breakdown between 145 ns and 155 ns. The gradual fall in current can be attributed to channel heating, which degrades mobility by lowering the mean scattering length. It can also be attributed to gradual burning of outer shells as well. Gradual burning and breakdown in less than 10 ns are attributed to kinetics of the sp^2 hybridized carbon atoms, which is decided by the Arrhenius relation.[23,24] Carbon

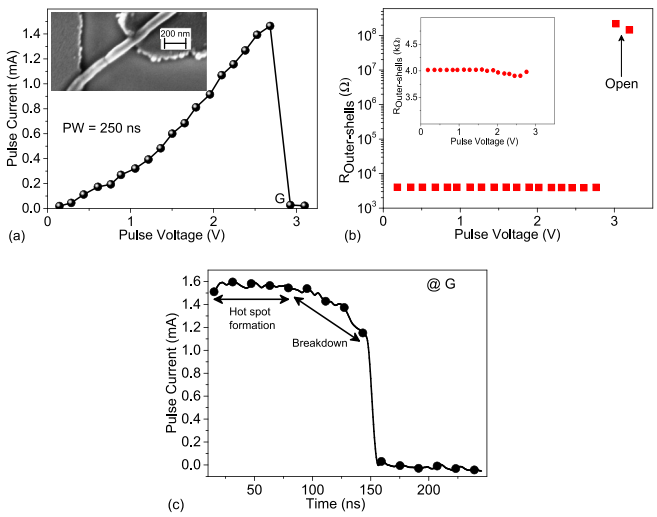

FIG. 4. (a) Pulse I-V characteristics of a 500 nm long suspended MWCNT, using a pulse width of 250 ns. The SEM image shows failure near the center, depicting a hot-spot at the center, which indicates diffusive transport before failure. (b) Change in the outer-shell resistance measured after each pulse. The tube breaks abruptly without showing any pulse-to-pulse degradation. The inset shows the same on a linear scale in the pre-breakdown regime. (c) Nano-second time resolved current waveform corresponding to point *G* in (a). The current waveform depicts three regions—(i) region in which current remains constant with time, (ii) gradual current degradation with time, and (iii) sharp breakdown.

atoms at defect sites on outer shells require smaller activation energy for oxidation; therefore, they get oxidized at relatively lower temperatures, which can be seen as gradual fall in current. As the channel temperature increases further, as per the Arrhenius equation, it gives rise to the rate of oxidation, which in turn results in a cascade of shell ablation and sharp failure within few nano-seconds.

As discussed in the beginning, thermal transport is associated with thermal diffusion time and hence the length of the tube. The contact and channel annealing reported above are found to have a strong dependence on time it takes to increase phonon population, and hence, it should be a strong function of the length of the tube as well. To validate this and arguments above, the change in the extent of annealing with the length is shown in Fig. 5. It clearly shows that annealing is a function of the length and the extent of annealing decreases with an increase in the length. In short tubes, the ballistic mode dominates the conduction as a result of which electron-phonon scattering and consequent hot-spot formation take place near the metal contacts. In contrast to this, scattering in the channel dominates within long tubes with diffusive transport. Increased phonon population across the tube results in desorption of surface adsorbents, while the same at the metal CNT interface improves the metal–carbon bonding and lowers the contact resistance. The former process decreases the resistance of the outermost shell only, while the latter decreases the contact resistance of the entire tube. Moreover, the longer tubes, due to longer diffusion time, require a relatively long period to anneal the channel and contacts. Consequently, compared to the long diffusive tube, the short ballistic tube shows a significant decrease in the resistance due to current annealing.

The device architecture discussed here features side-contacted tubes, where the outer-shell makes a physical contact with the metal, while the inner-shell participates in conduction via inter-shell tunneling. It is possible that adsorbents are trapped in the inner-shells, which in turn can suppress the tunneling and decrease the high-bias current. This is clearly captured in Fig. 6, where the low-bias resistance of both inner and outer shells show reduction at higher pulse voltages. It is interesting to note that the inner-shells show current-voltage behavior similar to the outer-shells, even after ablation or removal of the outer-shells. Such an annealing behavior indicates the presence of the tunneling barrier for inter-shell conduction and emphasizes the need for efficient metal-MWCNT contacts.

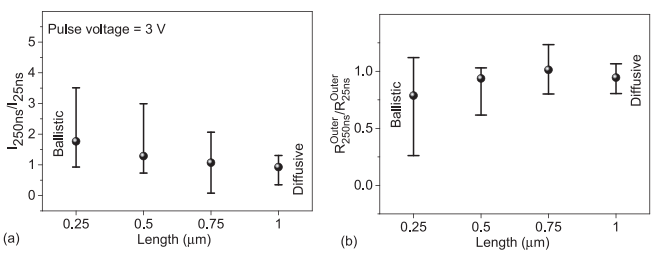

FIG. 5. (a) Ratio of pulse current at a pulse voltage of 3 V for pulse widths of 250 and 25 ns. (b) Ratio of the outer shell resistance extracted during 250 and 25 ns pulse tests. A total of 28 devices, 7 in each length set, were measured to perform the above extraction. The results of the measurement routine for one of the device are shown in Fig. S2 in the supplementary material.

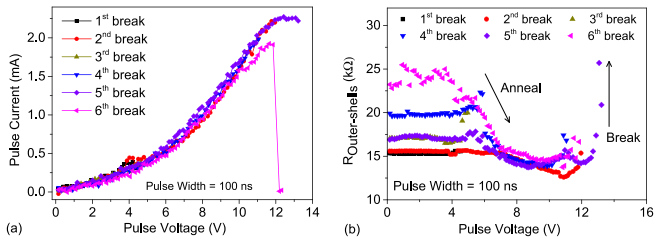

FIG. 6. Pulse IV characteristics (a) and pulse-annealing (b) of inner-shells of a MWCNT. The inner-shells independently show annealing, as indicated by reduction in the outer-shell resistance (b), which is followed by an increase in the overall conductance of the MWCNT, in spite of ablation of outer-shells (a). Note that the inner shells were made accessible by controlled damage of the outer-shells.

As a corollary to the observations presented so far, we extend our discussion to substrate-supported tubes. Besides having a higher technological relevance, as they are promising candidates for future interconnects, substrate-supported tubes are expected to have significant heat removal by the substrate. In such a case, if our argument above is true, as a result of relaxed channel heating and no contact heating, improvement in the channel property should be slow and minor. Figure 7(a) shows the pulse I-V characteristic of a 3 μm long substrate-supported tube using 50 and 100 ns long pulses. The pulse current and outer-shell resistance do not show any significant change with voltage and time (see Fig. S4 in the supplementary material), which validates our arguments above. Breakdown characteristics [Figure 7(b)] are also significantly different from suspended-tube architecture. The suspended-tube shows sudden breakdown without any saturation, while the substrate-supported tube breaks after saturation in current. We attribute this difference to the way heat dissipates in both the architectures. In contrast to suspended tubes, in substrate-supported tubes, phonons in the channel are coupled with surface phonon modes of the polar substrate.[25,26] This efficient heat exchange mechanism increases the thermal diffusivity across the CNT-SiO_2 interface. An increase in thermal diffusivity due to existence of extra phonon modes delays the formation of hot-spots and results in slow or no change in the tube's property.

In summary, a controlled method of investigating annealing and breakdown of MWCNTs using nano-second time resolved investigations has been developed, discussed,

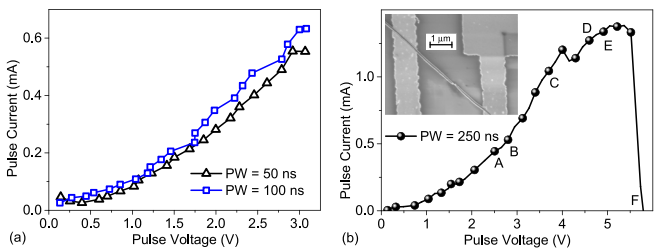

FIG. 7. Pulse I-V characteristics of a 3 μm long substrate-supported MWCNT. (a) Current for both 50 and 100 ns pulses increases non-linearly with voltage, indicating MWCNT behavior. (b) Breakdown is gradual and shows saturation before failure. The outer-shell resistance and transient waveforms are provided in Fig. S4 in the supplementary material. The inset in (b) shows the post-breakdown SEM image of a dielectric-supported MWCNT. Fail or breakdown away from the contact suggests diffusive transport, while a burn-spot on the substrate at the point of failure indicates the transfer of thermal energy from the MWCNT to the substrate.

and explored. The technique enables the investigation of electro-thermal transport at the time-scale comparable to the thermal diffusion time, which is of the order of few tens of nano-seconds. It was found that contact annealing precedes channel annealing and occurs predominantly for short ballistic tubes than long diffusive tubes. The change in the outer shell's resistance was found to be accumulative. The process, which caused non-destructive annealing by injecting nano-second time resolved thermal energy, is not only more reliable and controllable than other existing annealing methods but also gives insights into the process of annealing.

See supplementary material for the pulse I–V characteristics of suspended MWCNTs for a pulse width of 150 ns, the procedure adopted for the extraction of extent of annealing, and the pulse I–V characteristics of substrate-supported MWCNTs.

This work was financially supported by the Department of Science and Technology, Government of India (Project Grant No.: SB/S3/EECE/063/2014). A.M. thanks Professor K. K. Nanda (MRC, IISc) for his support in synthesizing the MWCNTs used in this work.

[1]S. Iijima, "Helical microtubules of graphitic carbon," Nature **354**, 56–58 (1991).
[2]H. J. Li, W. G. Lu, J. J. Li, X. D. Bai, and C. Z. Gu, "Multichannel ballistic transport in multiwall carbon nanotubes," Phys. Rev. Lett. **95**, 086601 (2005).
[3]B. Q. Wei, R. Vajtai, and P. M. Ajayan, "Reliability and current carrying capacity of carbon nanotubes," Appl. Phys. Lett. **79**, 1172–1174 (2001).
[4]E. Pop, S. Sinha, and K. E. Goodson, "Heat generation and transport in nanometer-scale transistors," Proc. IEEE **94**, 1587–1601 (2006).
[5]H. Maki, M. Suzuki, and K. Ishibashi, "Local change of carbon nanotube-metal contacts by current flow through electrodes," Jpn. J. Appl. Phys. **43**, 2027 (2004).
[6]Y. Woo, G. S. Duesberg, and S. Roth, "Reduced contact resistance between an individual single-walled carbon nanotube and a metal electrode by a local point annealing," Nanotechnology **18**, 095203 (2007).
[7]C. A. Santini, P. M. Vereecken, A. Volodin, G. Groeseneken, S. D. Gendt, and C. V. Haesendonck, "A study of joule heating-induced breakdown of carbon nanotube interconnects," Nanotechnology **22**, 395202 (2011).
[8]S. Chen, J. Y. Huang, Z. Wang, K. Kempa, G. Chen, and Z. F. Ren, "High-bias-induced structure and the corresponding electronic property changes in carbon nanotubes," Appl. Phys. Lett. **87**, 263107 (2005).
[9]M. Tsutsui, Y. K. Taninouchi, S. Kurokawa, and A. Sakai, "Bias-induced local heating effects on multi-walled carbon nanotube-au contacts," Jpn. J. Appl. Phys. **45**, 341 (2006).
[10]M. Tsutsui, Y.-K. Taninouchi, S. Kurokawa, and A. Sakai, "Electrical breakdown of short multiwalled carbon nanotubes," J. Appl. Phys. **100**, 094302 (2006).
[11]P. G. Collins, M. S. Arnold, and P. Avouris, "Engineering carbon nanotubes and nanotube circuits using electrical breakdown," Science **292**, 706–709 (2001).
[12]D. J. Yang, Q. Zhang, G. Chen, S. F. Yoon, J. Ahn, S. G. Wang, Q. Zhou, Q. Wang, and J. Q. Li, "Thermal conductivity of multiwalled carbon nanotubes," Phys. Rev. B **66**, 165440 (2002).
[13]W. Yi, L. Lu, Z. Dian-Lin, Z. Pan, and S. Xie, "Linear specific heat of carbon nanotubes," Phys. Rev. B **59**, R9015 (1999).
[14]G. F. Close, S. Yasuda, B. Paul, S. Fujita, and H.-S. P. Wong, "A 1 GHz integrated circuit with carbon nanotube interconnects and silicon transistors," Nano Lett. **8**, 706–709 (2008).
[15]B. Bourlon, C. Miko, L. Forró, D. C. Glattli, and A. Bachtold, "Determination of the intershell conductance in multiwalled carbon nanotubes," Phys. Rev. Lett. **93**, 176806 (2004).
[16]J. Moscatello, V. Kayastha, B. Ulmen, A. Pandey, S. Wu, A. Singh, and Y. K. Yap, "Surfactant-free dielectrophoretic deposition of multi-walled carbon nanotubes with tunable deposition density," Carbon **48**, 3559–3569 (2010).
[17]J. Moser, A. Barreiro, and A. Bachtold, "Current-induced cleaning of graphene," Appl. Phys. Lett. **91**, 163513 (2007).
[18]T. Yamada, T. Saito, M. Suzuki, P. Wilhite, X. Sun, N. Akhavantafti, D. Fabris, and C. Y. Yang, "Tunneling between carbon nanofiber and gold electrodes," J. Appl. Phys. **107**, 044304 (2010).
[19]A. Juutilainen, M. Ahlskog, and A. Volodin, "Measurements of tunneling conduction to carbon nanotubes and its sensitivity to oxygen gas," Phys. Rev. B **86**, 045405 (2012).
[20]A. Mishra and M. Shrivastava, "Remote joule heating assisted carrier transport in mwcnts probed at nanosecond time scale," Phys. Chem. Chem. Phys. **18**, 28932–28938 (2016).
[21]P. M. F. J. Costa, U. K. Gautam, Y. Bando, and D. Golberg, "Direct imaging of joule heating dynamics and temperature profiling inside a carbon nanotube interconnect," Nat. Commun. **2**, 421 (2011).
[22]H. Ulbricht, R. Zacharia, N. Cindir, and T. Hertel, "Thermal desorption of gases and solvents from graphite and carbon nanotube surfaces," Carbon **44**, 2931–2942 (2006).
[23]R. Brukh and S. Mitra, "Kinetics of carbon nanotube oxidation," J. Mater. Chem. **17**, 619–623 (2007).
[24]M. Shrivastava, N. Kulshrestha, and H. Gossner, "Esd investigations of multiwalled carbon nanotubes," IEEE Trans. Device Mater. Reliab. **14**, 555–563 (2014).
[25]S. V. Rotkin, V. Perebeinos, A. G. Petrov, and P. Avouris, "An essential mechanism of heat dissipation in carbon nanotube electronics," Nano Lett. **9**, 1850–1855 (2009).
[26]K. H. Baloch, N. Voskanian, M. Bronsgeest, and J. Cumings, "Remote joule heating by a carbon nanotube," Nat. Nanotechnol. **7**, 316–319 (2012).